analytical chemistry

Article

Cite This: *Anal. Chem.* 2019, 91, 13712−13719

pubs.acs.org/ac

Jungle on the Electrode: A Target-Induced Enzyme-Free and Label-Free Biosensor

Xian Chen,*[,†] Yaoze Liu,[†] Liming Xu,[†] Yang Wang,[†] Rui Li,[†] Pengming Sun,[‡] Zhenyu Lin,[†] and Huanghao Yang*[,†]

[†]College of Chemistry, Fuzhou University, Fuzhou 350116, People's Republic of China

[‡]Fujian Provincial Maternity and Children's Hospital, Affiliated Hospital of Fujian Medical University, Fuzhou 350001, People's Republic of China

Supporting Information

ABSTRACT: With the development of clinical medicine-related technologies, the detection of cancer biomarkers has become an essential method for cancer diagnosis. DNA self-assembly is a valuable approach to monitor low-abundance miRNA. Herein, we report a novel DNA jungle biosensor for target-induced enzyme-free and label-free ultrasensitive detection of miRNA-21 in biological samples. The method consists of two parts. The target catalyzes the assembly of the hairpin to form the backbone of the DNA jungle, and the auxiliary probes hybridize to form branches freely and undirectedly. The DNA jungle can be self-assembled seeded from a single target initiator, affording the potential for screening a single target molecule. Vitro assays show that the DNA jungle offers very high amplification efficiency and specificity, with a direct detection limit of 1 aM. This DNA jungle strategy can provide a useful platform for low-abundance biomarker detection for cell biology and diagnostics.

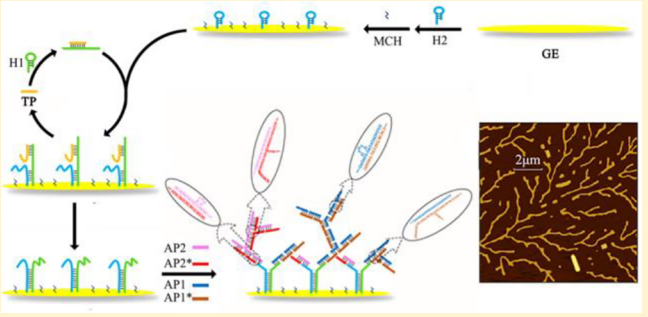

MicroRNAs (miRNAs) are sort of endogenous, single-stranded RNAs with lengths of 18−24 nucleotides, which play crucial roles in various biomedical processes, such as cellular proliferation differentiation and apoptosis.[1,2] For example, distinct miRNA expression patterns in cells are related to the occurrence, progression, and metastasis of various cancer types. Thus, miRNAs can be used as potential biomarkers[3] and drug targets for the prevention, treatment, and diagnosis of cancer.[4] The number of miRNAs detected in biological samples is vital for understanding the physiological functions of miRNAs, identifying cancer cells, and evaluating drug effects.

However, due to the fact of low abundance, small size, and high sequence similarity among family members, the development of simple and effective methods for miRNAs analyses remains a great challenge.[5] Up to now, scientists have proposed a variety of analytical methods to qualitatively and quantitatively detect miRNAs, such as polymerase chain reaction[9−11] and rolling circle amplification.[12−14] Although these methods can be used for the detection of exceedingly low levels of DNA, some inherent issues still cannot be avoided, for example, complex operations, costly polymerase, and tedious labels. Moreover, false-positives may sometimes happen during the amplification process. Some scientists use fluorescence to detect miRNAs, such as miRNA imaging.[6−8] Although this method can visually observe miRNAs, there are some defects, such as low sensitivity and needing complex operations or sophisticated instruments. There are other methods, such as molecular machines,[15−17] and so on.[18,19] These methods require subtle design or some new materials.

Fortunately, isothermal amplification methods that do not require precision instruments can effectively solve these problems. According to the mechanism of signal amplification, isothermal amplification can be divided into two major categories: nuclease-assisted and nonenzymatic reactions. Typically, nuclease-assisted methods are initiated by different nucleases to recycle the target, for instance, exonuclease,[20,21] endonuclease,[22−24] polymerase,[25,26] and the like.[27,28] Since enzymes usually act under very stringent conditions, such as pH and temperature, the enzyme-free reactions for amplifying miRNA have attracted the attention of more and more scientists, for example, hybridization chain reaction (HCR),[29−32] catalytic hairpin assembly (CHA),[33−36] and entropy drive.[37,38] These isothermal enzyme-free amplifications have several distinct advantages, such as simple operation, rapid detection, high sensitivity, high specificity, and low cost, making these methods ideal for highly sensitive biosensors.[39−42] However, most of these previous biosensors need three or more sets of auxiliary probes to form a DNA self-assembled structure with branches. The more branches, the

Received: July 3, 2019
Accepted: October 7, 2019
Published: October 7, 2019

DOI: 10.1021/acs.analchem.9b03004
Anal. Chem. 2019, 91, 13712−13719

Scheme 1. Schematic Diagram of the DNA Jungle Biosensor[a]

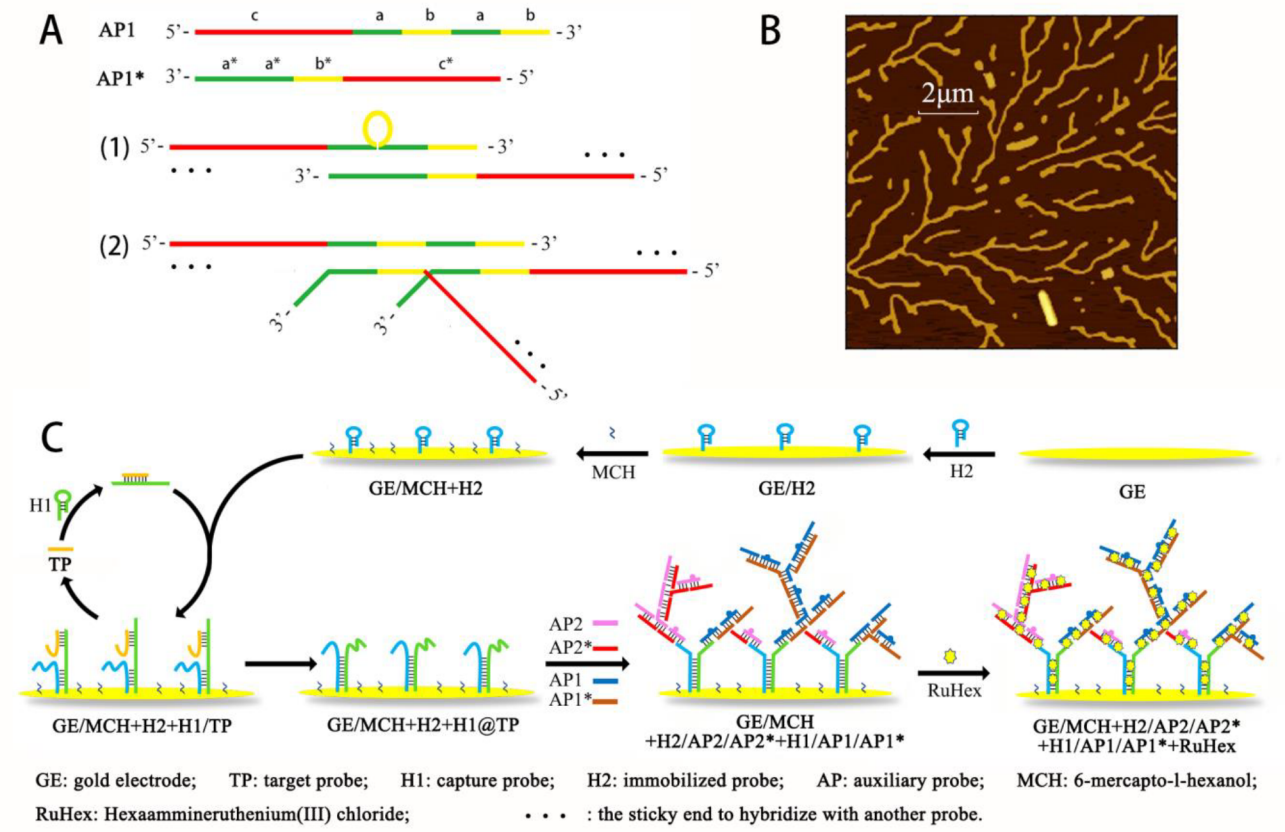

[a](A) Self-assembly of auxiliary probes in two ways, taking AP1 and AP1* as examples. (B) AFM images for DNA jungle on a mica substrate. (C) Construction of the DNA jungle biosensor.

more sets of auxiliary probes required, which results in intricate probe designing and self-assembled structures with limited branches. Therefore, it would be a new attempt to design as few as possible sets of auxiliary probes that can freely self-assemble and grow into complex DNA structures with an indefinite number of branches, just like a jungle assembled by DNA.

In this study, we design only two sets of auxiliary probes to self-assemble a DNA jungle on the electrode surface for ultrasensitive electrochemical detection. First of all, we specifically designed two hybridization modes for each set of auxiliary probes (AP). The self-assembly of the auxiliary probes can be described by taking AP1 and AP1* as examples. As shown in Scheme 1A, the base sequence of AP1 consists of five parts, which are c, a, b, a, and b, from the 5′ end to the 3′ end, respectively. The base sequence of AP1* consists of four parts, which are a*, a*, b*, and c*, from the 3′ end to the 5′ end, respectively. The sequences of parts a, b, and c can hybridize to sequences of parts a*, b*, and c*, respectively. Therefore, the part c of AP1 hybridizes to the complementary part c* of AP1* as usual. On the other hand, it is exquisitely designed that other parts of AP1 can hybridize to other parts of AP1* in two ways. One way is that a, a, and b of AP1 can hybridize to a*, a*, and b* of AP1* (Scheme 1A, (1)). The 3′ end of one AP1 hybridizes to the 3′ end of only one AP1*, and the hybrid product has two sticky ends, which are the 5′ end of AP1 and the 5′ end of AP1*. The base sequence and hybridizing pattern are shown in Figure S1A. The other way is that a and b of AP1 can hybridize to a* and b* of AP1* (Scheme 1A, (2)). Thus, the 3′ end of one AP1 can hybridize to the 3′ ends of two AP1* at the same time. The hybrid product has three sticky ends (the 5′ end of one AP1 and the 5′ ends of two AP1*) to hybridize with other probes. The corresponding base sequence and hybridizing pattern are shown in Figure S1B. Figure S1C,D shows the two hybridizing patterns of AP2 and AP2* as well. During the self-assembly of AP1 and AP1*, these two hybridization ways exist simultaneously and are randomly combined, and the sticky ends of these two hybrid products can continue to hybridize with other auxiliary probes, thereby self-assembling into branches of various forms, just like free-growing branches in the jungle. The situation is the same for AP2 and AP2*. Consequently, these two sets of auxiliary probes can self-assemble freely to be a lifelike DNA jungle on the electrode surface in the end (Scheme 1B).

Scheme 1C shows how this DNA jungle biosensor works. First of all, the immobilized probes (H2) are fixed on the surface of the gold electrode by the Au−S bond, and the capture probes (H1) are freely dispersed in the solution. In the absence of the target probe (TP), H1 and H2 are stably present as stem-loop structures, and no reaction occurs. When a TP (miRNA-21) is present, it can hybridize to an H1 and open the hairpin structure of the H1. One of the sticky ends of the H1 can hybridize to the sticky end of an H2. With the occurrence of competitive chain replacement, the TP will be replaced by the H2 and hybridize with another H1 to initiate another target circulation. Simultaneously, the H1 and the H2 hybridize on the electrode surface to form a double strand with two small tails. Next, two sets of particular sequences of DNA

DOI: 10.1021/acs.analchem.9b03004
Anal. Chem. 2019, 91, 13712−13719

auxiliary probes (AP1 and AP1*, AP2 and AP2*) are introduced and self-assembled to be a little jungle on the two small tails. As the target circulation progresses, more and more DNA tails appear on the surface of the electrode, and the DNA jungle also spreads. Finally, even if there is only one target, the DNA will grow freely and spread to be a vast jungle (Scheme 1B). In a word, this DNA jungle biosensor can achieve signal amplification twice by target circulation and infinite self-assembly of the auxiliary probes. Besides, RuHex can embed efficiently into the grooves of double-stranded DNA.[43] This character has been used to construct label-free electrochemical biosensors.[44] Accordingly, we use RuHex as the source of electrochemical signals.

EXPERIMENTAL SECTION

Materials and Reagents. Tris(hydroxymethyl) amino-meth-ane (Tris), hexaammineruthenium(III) chloride ($[Ru(NH_3)_6]^{3+}$, RuHex), 6-mercapto-l-hexanol (MCH), ethylenediaminetetraacetic acid (EDTA), and tris(2-carboxyethyl) phosphine hydrochloride (TCEP) were purchased from Sigma-Aldrich (U.S.A.). Al_2O_3 alumina slurry (0.3 μm, 0.05 μm) was purchased from Chenhua Instrument Co., Ltd. (Shanghai, China). Pure nitrogen (purity ≥ 99.99%) was purchased from Xinhang Industrial Gas Co., Ltd. (Fuzhou, China). Other chemicals employed were all of the analytical grade and purchased from Sinopharm Chemical Reagent Co. Ltd. (Shanghai, China). All solutions were prepared with ultrapure water obtained from a Milli-Q water purification system (Millipore Corp., Bedford, MA) with a resistivity of 18.2 MΩ·cm.

The buffers and solutions involved in this work were as follows: DNA immobilization buffer (10 mM Tris-HCl + 1 mM EDTA + 500 mM NaCl + 10 mM TCEP, pH 7.4), DNA hybridization buffer (10 mM Tris-HCl + 1 mM EDTA + 500 mM NaCl + 1 mM $MgCl_2$, pH 7.4), electrochemistry buffer (10 mM Tris-HCl, pH 7.4), MCH solution (2 mM MCH in water), and RuHex solution (50 μM $[Ru(NH_3)_6]^{3+}$ in 10 mM Tris-HCl, pH 7.4). All the oligonucleotides used in the present study were synthesized and purified by HPLC by Shanghai Shenggong Biotechnology Co. (Shanghai, China) and used without further purification. All the sequences (from 5′ to 3′) are shown in Table 1.

Human serum samples were provided by Fujian Provincial Maternity and Children's Hospital. The serum samples were centrifuged about 10 min at 1000 rpm, and then the supernatant was collected and stored at −20 °C.

Fabrication of the DNA Jungle Biosensor. The gold electrode (GE, shown in Scheme 1C, d = 2 mm) was immersed in a freshly prepared piranha solution (H_2SO_4:H_2O_2 = 3:1, v/v) for 30 min. The surface of the gold electrode was then washed with ultrapure water. The electrode was carefully polished to be a mirror surface with 0.3 and 0.05 μm alumina slurry and sonicated successively in water, ethanol, and water, to thoroughly remove the alumina slurry that may adhere to the electrode surface. Then, the electrode was electrochemically activated by cyclic voltammetry (CV) scanning in freshly prepared 0.5 M H_2SO_4 at a scan rate of 0.1 V/s^{-1} for 40 cycles, from −0.6 to +0.1 V. Continuous scanning until a stable cyclic voltammetry curve appeared. The cleaned electrode was thoroughly washed with a large amount of ultrapure water and dried under flowing nitrogen.

H1 and H2 probes were annealed in 95 °C water for 5 min and slowly cooled down to room temperature. 8 μL freshly prepared immobilization buffer containing 0.4 μM H2 was dripped on the gold electrode surface and incubated for 15 h to fix H2 to the electrode surface via Au−S bond (marked as GE/H2). After that, the surface of the electrode was washed with ultrapure water and dried with nitrogen. Then the electrode was incubated in 2 mM MCH for 1.5 h to block the unmodified sites on the surface. After washing with ultrapure water and drying with nitrogen, the working electrode (marked as GE/MCH+H2) was ready for use. Prepare the test sample containing 0.4 μM H1 and TP miRNA-21 (or target with mismatched base) of different concentration with hybridization buffer. A total of 8 μL of the sample was accurately dripped to the surface of the prepared working electrode (marked as GE/MCH+H2+H1/TP) and incubated at room temperature for 2 h (got a modified electrode GE/MCH+H2+H1@TP). The electrode surface should be covered with a little cap during incubation to maintain humidity, followed by being rinsing and drying.

A total of 10 μL of freshly prepared hybridization buffer containing 1 μM of AP1, AP1*, AP2, and AP2* was then dripped to the electrode surface (marked as GE/MCH+H2/AP2/AP2*+H1/AP1/AP1*) and incubated for 2 h at room temperature to allow the auxiliary probes to self-assemble and spread to be a DNA jungle. After that, the electrode was rinsed to remove nonspecifically adsorbed probes and dried with nitrogen.

Detection Method and Apparatus. Differential pulse voltammetry (DPV) and electrochemical impedance spectroscopy (EIS) were measured with CHI660 electrochemical workstation (Chenhua Instruments Co., Ltd., Shanghai, China). A three-electrode system consisting of the working electrode (the assembled gold electrode, d = 2 mm), Ag/AgCl reference electrode, and platinum counter electrode was used for all electrochemical measurements. DPV was measured in a 10 mM Tris-HCl (containing 50 mM RuHex) solution. The solution was deaerated by nitrogen for 15 min before the self-assembled DNA jungle electrode was immersed in it for 20 min. The positively charged RuHex in the solution would be adsorbed onto the negatively charged DNA phosphate backbone by electrostatic interaction. Then DPV scanning was performed with the scanning potential ranged from −0.6 to +0.1 V, pulse amplitude 0.05 V, and pulse width 0.05 s. EIS

Table 1. Sequence of Synthesized Oligonucleotides Probes Used in This Work[a]

oligonucleotide	sequence (from 5′ to 3′)
H1	GGCGGCTCAACATC *AGTCT GATAA GCTAC CATGT CCATG TGTAG ATAGC TTATC A* GACT
H2	HS$(CH_2)_6$TCAG *TGATA AGCTA TCTAC ACATG GACAT GGTAG CTTAT CAGAC T* CCATGTCCATGTGTAGA
AP1	GATGTTGAGCCGCC GATATA GTGTG GATATA GTGTG
AP1*	GGCGGCTCAACATC CACAC TATATC TATATC
AP2	ACAGA CGCGC ACAGA CGCGC TCTACACA TGGACATGG
AP2*	GCGCG GCGCG TCTGT CCATGTCCA TGTGTAGA
TP	UAGCUUAUCAGACUGAUGUUGA
1MT	UAGCUUAUCA**A**ACUGAUGUUGA
2MT	UAGCUUA**G**CAGACUG**G**UGUUGA
NC	CGAUAAUCGUUUACCGACCAUU

[a]The italics indicate the complementary parts of H1 and H2. The bold type bases are the mismatched bases of 1MT and 2MT.

DOI: 10.1021/acs.analchem.9b03004
Anal. Chem. 2019, 91, 13712−13719

was scanned in a 1 mM $Fe(CN)_6^{3-/4-}$ (containing 0.5 M KCl) solution with a frequency ranged from 0.1 Hz to 10 kHz.

RESULT AND DISCUSSION

Characterization of the DNA Jungle Sensing Platform. EIS measurements were performed to characterize the construction of the DNA jungle biosensor (Figure 1A). As shown in Figure 1A, curve a, there was only a relatively small electron-transfer resistance (Ret) on the bare electrode (GE), which indicated a fast charge-transfer process. After modified the electrode with H2, the Ret increased (Figure 1A, curve b) because the negative-charged phosphate skeletons of the H2 monolayer repelled $[Fe(CN)_6]^{3-/4-}$ from the electrode surface, suggesting the successful preparation of the modified electrode (GE/MCH+H2). After incubating H1 on the surface of GE/MCH+H2, only a slight change can be observed (Figure 1A, curve c), indicating that H1 and H2 were difficult to hybridize directly because of their beacon structure.

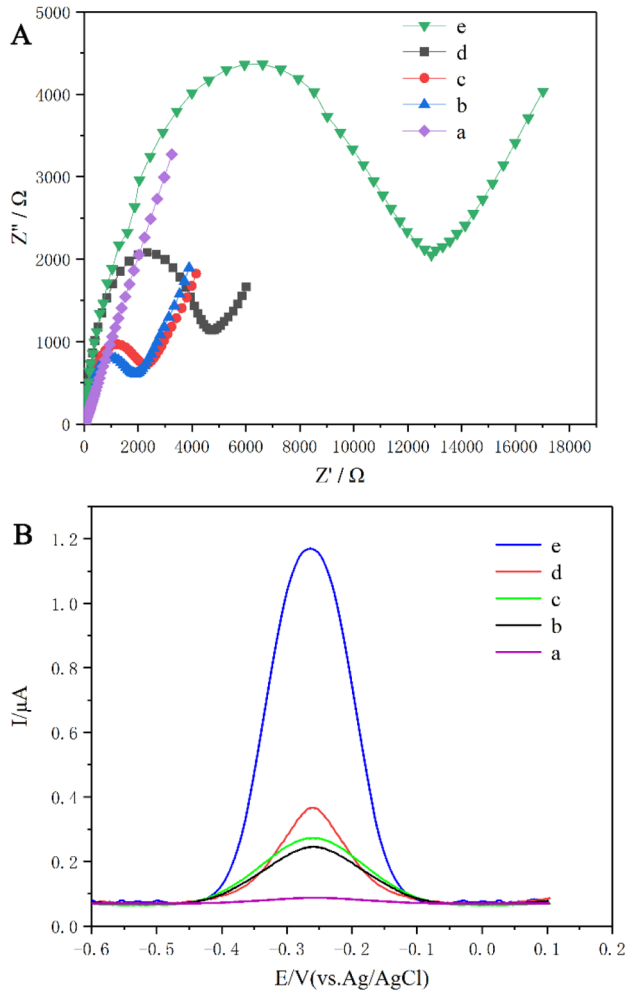

Figure 1. (A) EIS of the bare electrode GE (a), H2-modified electrode GE/MCH+H2 (b), GE/MCH+H2 incubated with 0.4 μM H1 (c), and GE/MCH+H2 incubated with a mixture of 10 pM TP, 0.4 μM H1 in the absence (d) and presence (e) of 1 μM AP1, AP1*, AP2, and AP2*. (B) DPV responses of the GE (a), H2-modified electrode GE/MCH+H2 (b), GE/MCH+H2 incubated with 0.4 μM H1 (c), and GE/MCH+H2 incubated with a mixture of 10 pM TP, 0.4 μM H1 in the absence (d) and presence (e) of 1 μM AP1, AP1*, AP2, and AP2*.

However, in the presence of TP miRNA-21, Ret continued to increase (Figure 1A, curve d), indicating that the phosphate backbone became longer, and more negative charges prevented electron transfer, which suggested that TP miRNA-21 initiated a strand displacement reaction between H1 and H2 on the surface of the electrode to form a hybrid strand with two tails (GE/MCH+H2+H1@TP).

If the buffer solution contained the two sets of auxiliary probes (AP1 and AP1*, AP2 and AP2*), they would hybridize to H1 and H2, respectively, and self-assemble to be a DNA jungle. As the DNA jungle grew on the surface of the electrode (GE/MCH+H2/AP2/AP2*+H1/AP1/AP1*), the negative charge increased significantly. Therefore, the electron transfer resistance enhanced further, and the Ret value multiplied (Figure 1A, curve e).

Figure 1B is the corresponding differential pulse voltammetry (DPV) response at different stages. RuHex cations can be quantitatively bound to the DNA phosphate backbone through electrostatic interactions and act as electrochemical indicator. The more RuHex bound to DNA, the higher the electrochemical signal produced. Before the bare electrode was modified, an ideal background was observed (Figure 1B, curve a). After H2 was immobilized on the surface of the gold electrode by the Au−S bond, only a small amount of RuHex was electrostatically adsorbed on the phosphate skeleton of the DNA, and thus, only a tiny reduction peak was produced (Figure 1B, curve b). After the incubation of H1 on the gold electrode, there was no significant change in the reduction peak, indicating that beacon H2 and beacon H1 could not hybridize (Figure 1B, curve c). However, in the presence of the target, it initiated a strand displacement reaction between H1 and H2 on the surface of the electrode to form a hybrid strand with two tails. As the phosphoric acid skeleton extended, more RuHex adsorbed, and the peak current increased (Figure 1B, curve d). When the two sets of auxiliary probes existed, AP1 would hybridize to H1, while AP2 would hybridize to H2. As DNA self-assembly progressed, a large amount of DNA jungle extended over the electrode surface, the electrostatically adsorbed RuHex increased, and the reduction peak multiplied (Figure 1B, curve e).

We used atomic force microscopy (AFM) imaging to visualize the morphology of the self-assembled DNA jungle to characterize the biosensing system further. A total of 10 μL of freshly prepared hybridization buffer was dripped (droplets containing 10 pM miRNA-21, 0.4 μM H1 and H2, and the two sets of auxiliary probes (1 μM)) onto the mica plate. After incubating for 120 min at room temperature and drying with nitrogen, a DNA jungle with many long, curled branches can be observed, as shown in Scheme 1B. Due to the random assembly of the auxiliary probes, the self-assembled products were polydisperse in size and branching efficiency, which made the product of self-assembly look like a vivid jungle growing on the mica plate, providing clear evidence for the construction of a DNA jungle in biosensor systems.

Optimization of Experimental Conditions. To achieve the best performance of the electrochemical biosensor, some vital experimental parameters were optimized. The 10 pM miRNA-21 was analyzed by the DPV peak current (I). The concentration of all the auxiliary probes was 1 μM. The time for self-assembly of auxiliary probes was 120 min. The density of H2 immobilized on the electrode was first studied by

DOI: 10.1021/acs.analchem.9b03004
Anal. Chem. 2019, 91, 13712−13719

controlling the concentration of H2 added on the electrode surface. The concentration of H1 was the same as the concentration of H2 used. The GE/MCH+H2 was incubated with H1 and miRNA-21 (TP) for 120 min. As shown in Figure 2A(a), as the H2 concentration increased, the peak current reached a maximum value at 0.4 μM and then decreased. Neither high nor low density of H2 was conducive to the construction of the sensor, because the low density reduced the probability of successful hybridization, and the high density produced steric hindrance to inhibit the reaction. Thus, 0.4 μM was selected as the optimized concentration of H2 for the fabrication of the electrochemical biosensor. We also studied the time of incubating H1 with miRNA-21 and H2. The concentrations of H1 and H2 were both 0.4 μM. As shown in Figure 2A(b), as the incubation time was extended from 15 to 120 min, the peak current gradually increased, and there was no significant change in the peak current after 120 min. Therefore, 120 min was chosen as the optimal incubation time of H1.

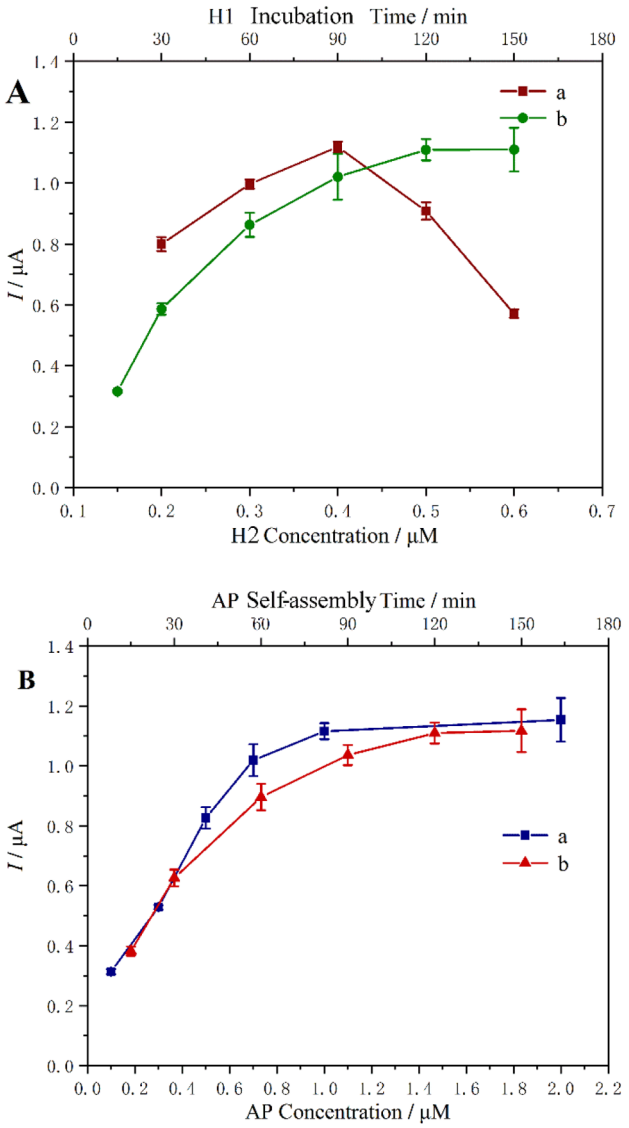

Figure 2. (A) (a) Effects of the concentrations of H2 for detection of 10 pM miRNA-21 in RuHex solution. Five different H2 concentrations (0.2, 0.3, 0.4, 0.5, and 0.6 μM) were used. (b) Effects of incubation time of 0.4 μM H1 for detection of 10 pM microRNA-21 in RuHex solution. The measurements were performed after 15, 30, 60, 90, 120, and 150 min of incubation time. (B) (a) Effects of the concentrations of auxiliary probes (AP1 and AP1*, AP2 and AP2*) for detection of 10 pM miRNA-21 in RuHex solution. All auxiliary probes were of the same concentration. Different concentrations of auxiliary probes were used (0.1, 0.3, 0.5, 0.7, 1.0, and 2.0 μM). (b) Effects of self-assembly time of 1.0 μM AP (0.4 μM H1 and H2) for detection of 10 pM miRNA-21 in RuHex solution. The measurements were performed after 15, 30, 60, 90, 120, and 150 min of self-assembly time. The error bars shown represent the standard deviation of three repeated measurements.

Figure 2B(a) shows the effect of different auxiliary probe concentrations (from 0.1 to 2.0 μM) on the signal values obtained by electrochemical detection of 10 pM miRNA-21. Four auxiliary probes of the same concentration were used in the assay, and the self-assembly time was 120 min. The peak current value also increased as the concentration of the auxiliary probes increassed from 0.1 μM to 1.0 μM. However, as the concentration of the auxiliary probe increased from 1.0 to 2.0 μM, the electrochemical signal did not increase significantly, which indicated that the self- assembled DNA jungle on the surface of the gold electrode had saturated after four auxiliary probes of 1.0 μM had been self-assembled for 120 min. Figure 2B(b) shows the effect of self-assembly time of auxiliary probes on the peak current. The concentration of all the auxiliary probes was 1 μM. As the self-assembly time was extended from 15 to 120 min, the peak current also gradually increased, and the peak current value no longer changed significantly when the self-assembly time was extended to 150 min. These results indicated that, after 120 min of self-assembly, the auxiliary probes on the electrode surface had all self-assembled to be a DNA jungle already. Therefore, the optimized DNA jungle self-assembly conditions were determined to be 1.0 μM of every auxiliary probe and 120 min of self-assembly time.

Assay Performance. We studied the analytical performance of the DNA jungle biosensor under optimal experimental conditions. The analysis was performed with the DPV peak current value as a signal. As shown in Figure 3A, in the concentration range of 1 aM to 10 pM, the peak current of DPV showed a different degree of increase with the increase of miRNA-21 concentration, which was related to the amount of electrostatic binding of RuHex cations to the DNA jungle on the electrode. As shown in Figure 3B, there was a good linear relationship between the DPV response and the logarithm of the miRNA-21 concentration, with the linear equation $Y = 0.112X + 2.2407$ and the correlation coefficient $R^2 = 0.9975$.

The directly measured detection limit toward the target is as low as 1 aM, providing superior detection sensitivity compared with most of the reported methods (Table S1).

Selectivity and Stability of Biosensors. In addition, the sensor has excellent specificity while achieving very satisfactory detection limits. In this work, four kinds of target sequences (see Table 1 for details) were chosen to study the selectivity of the biosensor, including miRNA-21 (TP), single-base mismatch target (1MT), two-base mismatch target (2MT), and noncomplementary sequence (NC). Figure 4 shows the peak currents of the blank and the four kinds of nucleic acid sequences. The concentration of miRNA-21 was 10 pM, while the concentrations of three other target sequences were 1 nM. Although the concentration of the three interfering substances tested was much larger than that of miRNA-21, the detection result of the sensor showed that the ratio of the peak current of

DOI: 10.1021/acs.analchem.9b03004
Anal. Chem. 2019, 91, 13712−13719

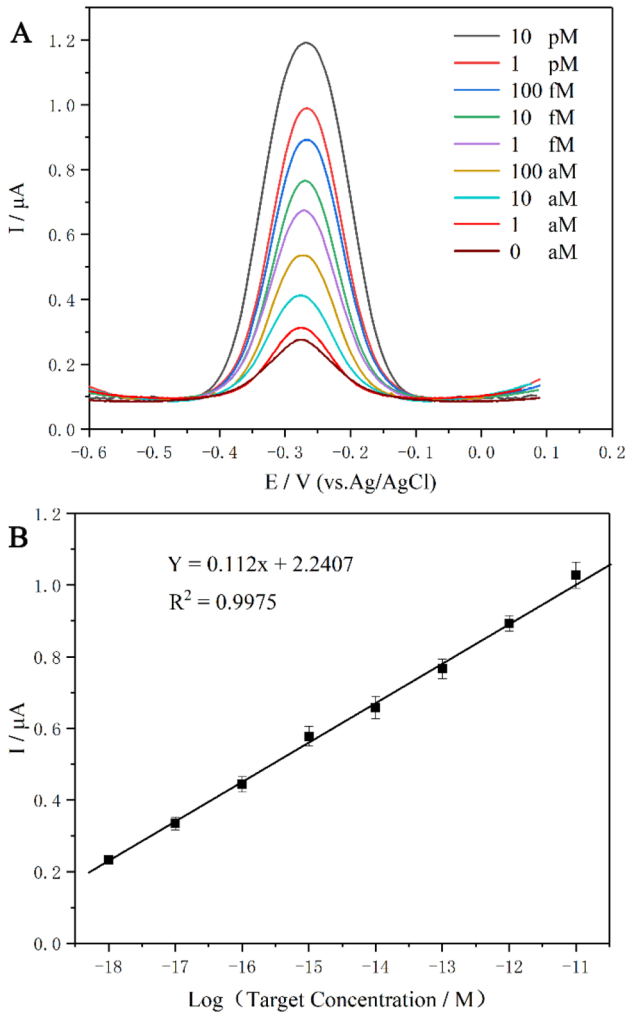

Figure 3. (A) DPV responses for different miRNA-21 concentrations: 0 aM, 1aM, 10 aM, 100 aM, 1 fM, 10 fM, 100 fM, 1 pM, and 10 pM. (B) The linear relationship between the peak current and the logarithm of the miRNA-21 concentration. The illustrated error bars represent the standard deviation of three repeated measurements.

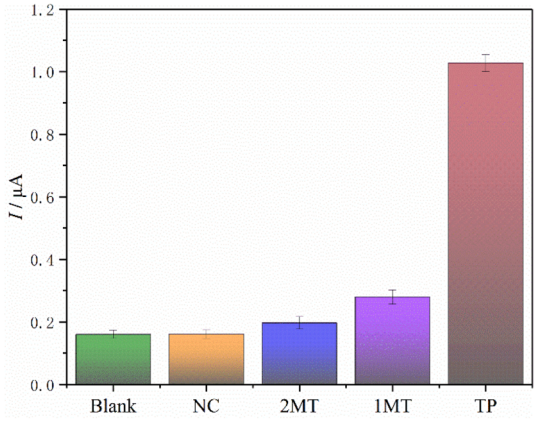

Figure 4. Bar chart of the DPV responses of the blank and the four various target sequences. The concentration of miRNA-21 (TP) was 10 pM. The concentrations of NC, 1MT, and 2MT are 1 nM. The illustrated error bars represent the standard deviation of three repeated measurements.

the miRNA-21 to that of the single base mismatch 1MT was about 4:1. The results indicated that this DNA jungle sensor produced a sensitive and specific response to the target miRNA-21. Gel electrophoresis imaging also demonstrated the excellent selectivity and specificity of the DNA jungle sensor (Figure S2).

The stability of the proposed biosensor was also verified by storing the established biosensor at 4 °C and measuring every 12 h. The results (Figure S3) showed that, after 72 h, the DPV response of the biosensor retained about 95.59% of its initial response, indicating the satisfactory stability of the proposed biosensor.

Challenged with Complex Samples. To further validate the sensor's detection performance for complex biological samples, we used this sensor to detect miRNA-21 in buffer and a 1:1 diluted human serum. As shown in Figure 5, under the same experimental conditions, when a DNA jungle biosensor was applied to detect a 1:1 diluted human serum sample, the signal was slightly reduced compared to the peak current observed in the buffer. This phenomenon may be due to complex components that interfere with the hybridization of the miRNA-21 and the capture probe in the serum. Besides, the signal of the blank serum sample is slightly larger than that of the blank buffer sample due to the nonspecific adsorption of complex biological components in the serum sample. However, DPV signals indicated that miRNA-21 concentrations could be detected as low as 1 aM even in 1:1 diluted human serum.

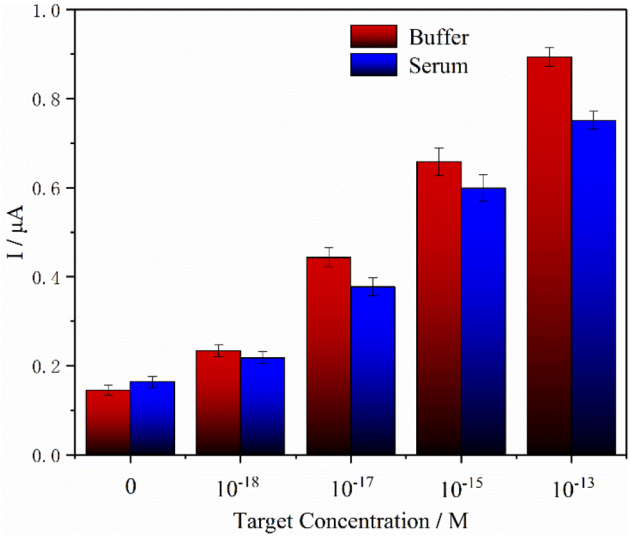

Figure 5. DPV peak currents obtained for the fabricated DNA jungle biosensor in buffer and 1:1 diluted serum of different miRNA-21 concentrations. The illustrated error bars represent the standard deviation of three repeated measurements.

In addition, various concentrations of miRNA-21 recovery tests have been performed in human serum samples provided by healthy individuals. As shown in Table S2, various concentrations of miRNA-21 (1, 10, and 1000 aM) were added to 1:1 diluted human serum samples, and the recoveries were 93%, 89.6%, and 93.56%, respectively. In view of these results, the recovery performance of the DNA jungle biosensor is fine, suggesting its great promise for miRNA-21 detection in complex biological samples.

Despite the effects of various complex components of biological samples, the DNA jungle biosensor still exhibited

DOI: 10.1021/acs.analchem.9b03004
Anal. Chem. 2019, 91, 13712−13719

superior performance. To the best of our knowledge, this detection system is the most sensitive one compared to other reported electrochemical biosensors, which demonstrates the promising advantage of DNA jungle biosensors in real physiological media.

CONCLUSION

We designed two sets of auxiliary probes sophisticatedly to construct a DNA jungle biosensor for specific detection of miRNA-21 in complex biological samples. This method avoids the use of an enzyme or sophisticated equipment and does not require any marking. The free growth of a large number of DNA jungles requires only two sets of auxiliary probes, avoiding the adverse effects of excessive types of auxiliary probes. Significantly, the proposed biosensor can detect miRNA-21 down to 1 aM in 1:1 diluted human serum directly, with similar sensitivity to PCR and high selectivity to distinguish mismatch targets. This result means that six copies of miRNA-21 can be detected directly in 10 μL of biological sample with the DNA jungle biosensor. According to the principle of the experiment, if another miRNA target needs to be detected, the detection can be achieved by simply changing the corresponding complementary sequence of the H1 loop. This design concept makes this sensor a promising general method for ultrasensitive detection of miRNAs. This study opens a promising approach to develop enzyme-free and ultrasensitive-electrochemical bioassays, holding great potential for early diagnosis in gene-related diseases.

ASSOCIATED CONTENT

Supporting Information

The Supporting Information is available free of charge on the ACS Publications website at DOI: 10.1021/acs.analchem.9b03004.

Auxiliary probes self-assembly; gel electrophoresis; stability investigation; comparison with other reported methods; and recovery tests (Figures S1−S3 and Tables S1 and S2) (PDF)

AUTHOR INFORMATION

Corresponding Authors

*Tel.: +86 591 22866234. E-mail: xchen_fzu@126.com.
*E-mail: hhyang@fzu.edu.cn.

ORCID

Xian Chen: 0000-0003-4301-1909
Zhenyu Lin: 0000-0001-7890-6812
Huanghao Yang: 0000-0001-5894-0909

Author Contributions

X.C.: Conceptualization, methodology, and writing, reviewing, and editing. Y.L.: Investigation, methodology, and writing, reviewing and editing. L.X.: Investigation. Y.W.: Investigation. R.L.: Investigation. P.S.: Investigation. Z.L.: Writing, reviewing, and editing. H.-H.Y.: Supervision.

Notes

The authors declare no competing financial interest.

ACKNOWLEDGMENTS

This work was financially supported by the Department of Education, Fujian Province, China (Grant No. JK2017006); the National College Student Innovation and Entrepreneurship Training Program Project Fund (Grant No. 201910386009), China; and the National Natural Science Foundation of China, China (Grant No. 21575027).

REFERENCES

(1) Gebert, L. F. R.; MacRae, I. *Nat. Rev. Mol. Cell Biol.* **2019**, *20*, 21−37.
(2) Bartel, D. P. *Cell* **2004**, *116*, 281−297.
(3) Esquela-Kerscher, A.; Slack, F. *Nat. Rev. Cancer* **2006**, *6*, 259−269.
(4) Grosshans, H.; Filipowicz, W. *Nature* **2008**, *451*, 414−416.
(5) He, L.; Hannon, G. *Nat. Rev. Genet.* **2004**, *5*, 522−532.
(6) Sun, Y. D.; Shi, L.; Wang, Q. W.; Mi, L.; Li, T. *Anal. Chem.* **2019**, *91*, 3652−3658.
(7) Liang, C. P.; Ma, P. Q.; Liu, H.; Guo, X. G.; Yin, B. C.; Ye, B. C. *Angew. Chem., Int. Ed.* **2017**, *56*, 9077−9081.
(8) Yue, S. Z.; Song, X. Y.; Song, W. L.; Bi, S. *Chem. Sci.* **2019**, *10*, 1651−1658.
(9) Yu, C. Y.; Yin, B. C.; Wang, S. L.; Xu, Z. G.; Ye, B. C. *Anal. Chem.* **2014**, *86*, 7214−7218.
(10) Dong, J.; Chen, G. Y.; Wang, W.; Huang, X.; Peng, H. P.; Pu, Q. L.; Du, F.; Cui, X.; Deng, Y.; Tang, Z. *Anal. Chem.* **2018**, *90*, 7107−7111.
(11) Zhou, M. X.; Teng, X. C.; Li, Y.; Deng, R. J.; Li, J. H. *Anal. Chem.* **2019**, *91*, 5295−5302.
(12) Fan, T. T.; Mao, Y.; Sun, Q. S.; Liu, F.; Lin, J. S.; Liu, Y. J.; Cui, J. W.; Jiang, Y. Y. *Cancer Sci.* **2018**, *109*, 2897−2906.
(13) Wang, S.; Lu, S. S.; Zhao, J. H.; Ye, J.; Huang, J. S.; Yang, X. R. *Biosens. Bioelectron.* **2019**, *126*, 565−571.
(14) Chen, J.; An, T. X.; Ma, Y. J.; Situ, B.; Chen, D. P.; Xu, Y. Z.; Zhang, L.; Dai, Z.; Zou, X. Y. *Anal. Chem.* **2018**, *90*, 859−865.
(15) Chen, T. S.; Chen, Y. Y.; Chen, H. N.; Zhang, F.; Zhang, Q. Q.; Chen, G. F.; Zhu, X. L. *Nano Res.* **2019**, *12*, 1055−1060.
(16) Zhang, P.; Jiang, J.; Yuan, R.; Zhuo, Y.; Chai, Y. Q. *J. Am. Chem. Soc.* **2018**, *140*, 9361−9364.
(17) Peng, L. C.; Zhang, P.; Chai, Y. Q.; Yuan, R. *Anal. Chem.* **2017**, *89*, 5036−5042.
(18) Liu, J. L.; Tang, Z. L.; Zhang, J. Q.; Chai, Y. Q.; Zhuo, Y.; Yuan, R. *Anal. Chem.* **2018**, *90*, 5298−5305.
(19) Chen, Z. X.; Peng, Y. J.; Cao, Y.; Wang, H.; Zhang, J. R.; Chen, H. Y.; Zhu, J. J. *Nano Lett.* **2018**, *18*, 3759−3765.
(20) Ding, B. M.; Liu, C. G.; Wu, Q. H.; Wang, Y.; Li, L.; Yang, H. L. *Anal. Sci.* **2018**, *34* (3), 259−261.
(21) Chen, Y. H.; Duong, H. T. T.; Wen, S. H.; Mi, C.; Zhou, Y. Z.; Shimoni, O.; Valenzuela, S. M.; Jin, D. Y. *Anal. Chem.* **2018**, *90*, 663−668.
(22) Mittal, S.; Thakur, S.; Mantha, A. K.; Kaur, H. *Biosens. Bioelectron.* **2019**, *124−125*, 233−243.
(23) McVey, C.; Huang, F.; Elliott, C.; Cao, C. *Biosens. Bioelectron.* **2017**, *92*, 502−508.
(24) Pu, Q. L.; Li, J. L.; Qiu, J. H.; Yang, X. H.; Li, Y.; Yin, D.; Zhang, X. Y.; Tao, Y. Y.; Sheng, S. C.; Xie, G. M. *Biosens. Bioelectron.* **2017**, *94*, 719−727.
(25) Chen, Z. Q.; Wang, C.; Hao, L. J.; Gao, R.; Li, F.; Liu, S. F. *Biosens. Bioelectron.* **2019**, *128*, 104−112.
(26) Peng, K. F.; Xie, P.; Yang, Z. H.; Yuan, R.; Zhang, K. Q. *Biosens. Bioelectron.* **2018**, *102*, 282−287.
(27) Lv, Y. Q.; Chen, S. Y.; Shen, Y. F.; Ji, J. J.; Zhou, Q.; Liu, S. Q.; Zhang, Y. J. *J. Am. Chem. Soc.* **2018**, *140*, 2801−2804.
(28) Liu, X. F.; Zhang, H.; Qin, S. Y.; Wang, Q.; Yang, X. H.; Wang, K. M. *Biosens. Bioelectron.* **2019**, *129*, 87−92.
(29) Wang, Y.; Bai, J. L.; Huo, B. Y.; Yuan, S.; Zhang, M.; Sun, X.; Peng, Y.; Li, S.; Wang, J.; Ning, B.; Gao, Z. X. *Anal. Chem.* **2018**, *90*, 9936−9942.
(30) Chen, X.; Hong, C. Y.; Lin, Y. H.; Chen, J. H.; Chen, G. N.; Yang, H. H. *Anal. Chem.* **2012**, *84*, 8277−8283.
(31) Shi, X. M.; Fan, G. C.; Tang, X. Y.; Shen, Q. M.; Zhu, J. J. *Biosens. Bioelectron.* **2018**, *109*, 190−196.
(32) Guo, W. J.; Wu, Z.; Yang, X. Y.; Pang, D. W.; Zhang, Z. L. *Biosens. Bioelectron.* **2019**, *131*, 267−273.

DOI: 10.1021/acs.analchem.9b03004
Anal. Chem. 2019, 91, 13712−13719

(33) He, C. L.; Wang, M. Q.; Sun, X. B.; Zhu, Y.; Zhou, X.; Xiao, S. Y.; Zhang, Q. J.; Liu, F. N.; Yu, Y.; Liang, H. J.; Zou, G. *Biosens. Bioelectron.* **2019**, *129*, 50−57.
(34) Wang, S.; Lu, S. S.; Zhao, J. H.; Ye, J.; Huang, J. S.; Yang, X. R. *Biosens. Bioelectron.* **2019**, *126*, 565−571.
(35) Karunanayake Mudiyanselage, A. P. K. K.; Yu, Q. K.; Leon-Duque, M. A.; Zhao, B.; Wu, R.; You, M. X. *J. Am. Chem. Soc.* **2018**, *140*, 8739−8745.
(36) Liu, Z.; Lei, S.; Zou, L.; Li, G. P.; Xu, L. L.; Ye, B. X. *Biosens. Bioelectron.* **2019**, *131*, 113−118.
(37) Zhang, D. Y.; Turberfield, A. J.; Yurke, B.; Winfree, E. *Science* **2007**, *318*, 1121−1125.
(38) Thaner, R. V.; Kim, Y.; Li, T. I. N. G.; Macfarlane, R. J.; Nguyen, S. T.; Olvera de la Cruz, M.; Mirkin, C. A. *Nano Lett.* **2015**, *15*, 5545−5551.
(39) Wen, J. L.; Chen, J. H.; Zhuang, L.; Zhou, S. G. *Biosens. Bioelectron.* **2016**, *79*, 656−660.
(40) Yu, S.; Wang, Y. Y.; Jiang, L. P.; Bi, S.; Zhu, J. J. *Anal. Chem.* **2018**, *90*, 4544−4551.
(41) Liu, Y.; Wei, Y. D.; Cao, Y. J.; Zhu, D. B.; Ma, W. G.; Yu, Y.; Guo, M. L. *Biosens. Bioelectron.* **2018**, *117*, 830−837.
(42) Chang, C. C.; Chen, C. Y.; Chuang, T. L.; Wu, T. H.; Wei, S. C.; Liao, H. E.; Lin, C. W. *Biosens. Bioelectron.* **2016**, *78*, 200−205.
(43) Carter, M. T.; Bard, A. J. *Bioconjugate Chem.* **1990**, *1*, 257−263.
(44) Zhang, Y.; Wang, L. X.; Luo, F.; Qiu, B.; Guo, L. H.; Weng, Z. Q.; Lin, Z. Y.; Chen, G. N. *Chem. Commun.* **2017**, *53*, 2910−2913.

DOI: 10.1021/acs.analchem.9b03004
Anal. Chem. 2019, 91, 13712−13719